scientific reports

Check for updates

OPEN

Synthesis of bimetallic nanoparticles loaded on to PNIPAM hybrid microgel and their catalytic activity

Mohib Ullah Kakar[1,2], Khakemin Khan[3], Muhammad Akram[4], Rokayya Sami[5]✉, Ebtihal Khojah[5], Imran Iqbal[6], Mahmoud Helal[7], Abdul Hakeem[2], Yulin Deng[1] & Rongji Dai[1]✉

This study was designed to preparecarboxyl-functionalized poly (N-isopropylacrylamide) PNIPAM microgels having excellent catalytic properties.Recently, researchers are trying to fabricate cost effective and efficient hybrid catalytic materials for the synthesis of nitrogenous compounds along with enhanced optical properties. For the same motive, synthesis of carboxyl-functionalized PNIPAM microgels was performed by using polymerization of soap-free emulsion of N-isopropyl acrylamide, which is NIPAM along with acrylic acid (AA). The thiol group was introduced through the imide bond mediated by carbodiimide, between carboxyl-functionalized microgels through carboxyl group and aminoethanethiol (AET). Copper, Palladium and Cu/Pd nanoparticles were incorporated successfully into thiol-functionalized PNIPAM microgels through metals thiol linkage. The synthesized microgels and hybrid encompassing metallic nanoparticles were characterized in detail by using Transmission electron microscopy (TEM), Scanning electron microscopy (SEM), X-ray diffraction (XRD), X-ray photoelectron (XPS) and Fourier transformed infrared spectroscopy for structural interpretation. The thermal properties of the pure and hybrid microgels were inspected by TG analysis. The prepared nanocomposites PNIPAM-Cu, PNIPAM-Pd and PNIPAM-Cu/Pd exhibited decent catalytic properties for the degradation of 4-Nitrophenol and methylene blue, but the bimetallic Cu/Pd have remarkable catalytic properties. The catalytic reaction followed pseudo-first-order reaction with rate constants 0.223 min^{-1}, 0.173 min^{-1} for 4-Nitrophenol and methylene blue in that order. In this study,we were able to establish that Cu/Pd hybrid is an efficient catalyst for 4-Nitrophenol and methylene blue as compared to its atomic analogue.

Metallic nanoparticles have charmed attraction for few decades owing to their abundance and variety of applications in catalysis[1], medicine[2], bio/imaging[3], sensors[4], and electronics[5]. Due to their high surface area and greater surface energy, nanoparticles (NPs) showed prominent catalytic activities like CO oxidation[6] for nucleation of carbon nanotubes (CNTs)[7], dehydrogenation of alcohol[8] as well as electro-oxidation of formic acids[9]. Due to the high surface energy and van der Waal forces, NPs can aggregate, which reduces the surface area as well as catalytic activities. Therefore, metal NPs can be stabilized by using suitable additives like hydrogels[10], dendrimers[11], micelles of block copolymers[12] and gutta-percha particles[13].

For the specific characteristic properties of nanocomposites, nanoparticles such as carbon-based[14], ceramic[15], and metallic nanoparticles[16] can be incorporated/implanted within the hydrogel network[10]. Nanocomposite hydrogels or hybrid hydrogels (highly hydrated polymeric networks) are either physically or covalently cross-linked with nanoparticles[17–19]. Nanocomposite hydrogels can be constructed in the presence of microgel

[1]Beijing Key Laboratory for Separation and Analysis in Biomedicine and Pharmaceutical, Beijing Institute of Technology (BIT), Beijing 100081, People's Republic of China. [2]Faculty of Marine Sciences, Lasbela University of Agriculture, Water and Marine Sciences (LUAWMS), Uthal, Balochistan, Pakistan. [3]Department of Chemistry, Hazara University, Khyber Pakhtunkhwa, Pakistan. [4]Institute for Synthetic Biosystem, School of Chemistry and Chemical Engineering, Beijing Institute of Technology, Beijing 100081, People's Republic of China. [5]Department of Food Science and Nutrition, College of Sciences, Taif University, P.O. 11099, Taif 21944, Saudi Arabia. [6]Department of Information and Computational Sciences, School of Mathematical Sciences and LMAM, Peking University, Beijing 100871, People's Republic of China. [7]Department of Mechanical Engineering, Faculty of Engineering, Taif University, Taif, Saudi Arabia. ✉email: rokaya.d@tu.edu.sa; dairongji@bit.edu.cn

stabilizers with enhanced physical, chemical, electrical, and biological properties like the hybridization of organic and inorganic nanoparticles including surface Plasmon resonance (SPR) and photoluminescence, etc[20–22]. For the in-situ synthesis of nanocomposite microgel and NPs, hydrogels are primary carrier due to their hydrating ability for catalytic reactions as well as recycling ability without losing the NPs. The functional groups of hydrogel networks like $–SO_3H$, –SH, –OH, $–NH_2$, and –COOH attract metal ions with electrostatic interactions. It helps to stabilize and reduce the hydrogel through a suitable reducing agent. Therefore, hydrogels are used as real reactors for the in-situ synthesis of metal NPs to avoid aggregation. In recent years, polymer hydrogels have been investigated as an efficient and real reactor for in-situ synthesis of metallic NPs for the decomposition of various aromatic pollutants and dyes[23–25]. Most of the researchers have focused on metallic, nonmetallic and semiconductor nanoparticles, e.g. Au[26], Ag[27], Pd[28], Co[29], ZnO[30], CeO_2[31], TiO_2[32] etc. It is reported in most of the literature that Au, Ag and Pd nanoparticles were used to reduce 4-NP to 4-aminophenol[33–36]. The catalytic activities of gold, silver and palladium nanoparticles, impregnated in microgels, were studied[37–39].

Bimetallic nanoparticles of two different metals have become very popular in recent years due to their unique and enhanced catalytic properties as compared to their monometallic analogues[40–42]. The catalytic properties of Pd in any bimetallic catalysts are greater as compared to other bimetallic except Pd as one of its components[26,43,44]. Therefore, Pd based bimetallic catalysts are considered as promising candidates for the degradation of different organic and environmental pollutants. For example, Pd/Au[45], Pd/Ni[46], Pd/Pt[44] and Pd/Cu[47] are investigated as prominent bimetallic materials for various applications.

In this study, we have reported thiol-functionalized microgels to stabilize Cu, Pd, and Cu/Pd bimetallic NPs and applied them to degrade 4-Nitrophenol and methylene blue in which the bimetallic NPs showed efficient catalytic properties. Therefore, we suggest, Cu/Pd bimetallic based microgels are promising catalysts for the degradation of environmental pollutants.

Experimental

Materials. N-Isopropyl acrylamide (NIPAM) purchased from Sigma Aldrich, Inc. and purified by recrystallization. For recrystallization purpose, n-hexane was used as a solvent and material was vacuum dried. Reduced nitrogen pressure was used for refinement of acrylic acid (AA). Then deionized water was used for recrystallisation and distillation of Potassium per sulfate (KPS). *N*,*N*-Methylene bisacrylamide (MBA, Alfa Aesar), 1-ethyl-3-(3-dimethylaminopropyl) carbodiimide hydrochloride (EDAC, Alfa Aesar, 98%), Copper nitrate trihydrate Cu $(NO_3)_2{\cdot}3H_2O$ and $PdCl_2$. 2-aminoethanethiol (AET, RED chemical), ascorbic acid and Hydrazine (98.0%) were used as received. All experiments were performed by using double distilled water.

Carboxyl-functionalized PNIPAM microgels synthesis. We synthesized carboxyl-functionalized microgels through soap-free emulsion polymerization technique by mixing N-Isopropyl acrylamide (NIPAM) and acrylic acids. For this purpose, round bottom flask (three necked, 500 ml capacity) was used having a mechanical stirrer equipped with a nitrogen inlet. The composition of the microgels was as 2 g NIPAM, 0.2 g AA monomer, a cross linker MBA (0.2 g) and KPS as an initiator (0.1 g) with deionized water (300 mL) was stirred with (300 rpm) and continuous supply of nitrogen gas for 30 min. Polymerization was induced by increasing the temperature up to 70 °C, time spanning over 6 h. Purification of these prepared microgels was done by dialysis using the deionized water for 3 days. The water was replaced frequently after 10 h.

Preparation of thiol-functionalized PNIPAM microgels. Thiol-functionalized PNIPAM microgels were prepared. This preparation was based on the formation of amid bond between the functional group of microgel and amine group of AET. 100 mL of carboxyl-functionalized PNIPAM microgel aqueous dispersion and 0.2 mL AET aqueous solution (20 mL) were charged into three-necked round bottom flask (250 mL capacity) and agitated at (200 rpm) at 20 °C for 10 min. Then, 20 mL of 0.46 M EDAC aqueous solution was added and the pH was adjusted to 6.1 by using 0.2 M aqueous HCl. This reaction performed at 20 °C for 2 h under constant stirring. Excess amounts of unreacted chemicals AET were removed, and the obtained thiol-functionalized PNIPAM microgels dispersion were further dialyzed against deionized water for purification.

In situ synthesis of metals nanoparticles in PNIPAM microgels. In-situ synthesis of metal nanoparticles in microgels network, 10 mL of 50 ppm metal salts Cu $(NO_3)_2{\cdot}3H_2O$, $PdCl_2$ was added to 10 mL already prepared microgels which were further diluted by adding 15 mL deionized water respectively. With constant stirring and refluxing at 120 °C, 0.5 mL ascorbic acid (0.05 M) was added. Then 2 mL of NaOH (0.6 M) was added to the solution after further stirring for 20 min. Finally, a 0.5 mL volume (0.05 M) of $N_2H_4$was added and the color of the colloidal solution changed which indicated the formation of metals hybrid nanoparticles.

Preparation of PNIPAM/Bimetallic Cu/Pd Hybrid microgels. 10 mL of (0.05 M) $PdCl_2$ was used to prepare the Pd nanoparticles, as described by Turkevich[57]. According to this method, 10 mL of (0.05 M) $PdCl_2$ was added to 10 mL of prepared microgels which were further diluted by adding 15 mL of deionized water. 0·5 mL ascorbic acid was added after stirring for 20 min and then 10 mL Cu $(NO_3)_2{\cdot}3H_2O$ (0.05 M) was added. 2 mL NaOH (0.6 M) was added drop wise and we adjusted the pH of the above colloidal solution to 8.5 with continuous stirring for further 30 min. In the end, 0·5 mL volume (0·05 M) of $N_2H_4$was added and the color of colloidal solution became dark muddy which showed the formation of bimetallic hybrid nanoparticles.

4-Nitrophenol and methylene blue reduction, catalyzed by PNIPAM-K hybrid microgels. Thermally tunable catalytic property of bimetallic based PNIPAM microgels was explored 4-Nitrophenol (4-NP)

along with methylene blue reduction in the presence of NaBH4 at different range of temperatures. The process was done into a quartz cell for UV–Vis spectroscopy. 1 mL of 4-NP and 1 mL methylene blue aqueous solution (0.1 mM) was separately mixed with 2 mL of 20 mM $NaBH_4$ aqueous solution, then added into a quartz cell and test it at given temperature. All at once, the PNIPAM/Cu and PNIPAM/Pd hybrid microgels latex were put in a water bath for acquiring the testing temperature. Afterwards, 0.5 mL of PNIPAM/Cu and Pd latex (0.06 mg/mL) was placed in thee quartz cell and then UV–Vis spectra was obtained after each set interval of time. The reduction rate constant for 4-Nitrophenol was determined by computing the decrease in intensity at 400 nm and for Methylene blue at 650 nm by various catalytic agents. A calibration curve was formed at 400 nm for 4-Nitrophenol and 650 for methylene blue to find the concentration of the reagents. The reduction rates of 4-Nitrophenol and methylene blue were calculated at four different temperatures i.e. 30 °C, 32 °C, 34 °C and 36 °C. During this study, every obtained data was repeated three times for the sake of accuracy.

Catalytic properties of PNIPAM based bimetallic Cu/Pd by reducing 4-Nitrophenol and methylene blue. Similarly, the thermal tunable catalytic properties of PNIPAM based bimetallic copper and palladium alloy were studied by reducing 4-Nitrophenol and methylene blue at a given range of temperature. One mL of each methylene blue and 4-Nitrophenol, 0.1 mM aqueous solution separately mixed with 10 mM $NaBH_4$ aqueous solution (1 mL). The solution was then adjusted to the given temperature. Along with this, the PNIPAM-Cu/Pd hybrid microgels were placed for 10 min in the water bath for acquiring the testing temperature. Later on, 0.2 mL of PNIPAM-Cu/Pd hybrid microgels latex (0.06 mg/mL) was also added into the quartz cell, and then at each set time interval, UV–Vis spectra was taken without any delay. . The reduction rate constant for nitrophenol was determined by computing the decrease in intensity at 400 nm and for methylene blue at 650 nm by various catalytic agents. A calibration curve was formed at 400 nm for 4-Nitrophenol and 650 nm for methylene blue in order to find the concentration of the reagents. The rate of reduction of 4-Nitrophenol and methylene blue were calculated at four different temperatures i.e. 30 °C, 32 °C, 34 °C and 36 °C. During this study, every obtained data was repeated three times for the sake of accuracy.

Characterization. *Fourier transform infrared spectroscopy.* Fourier transform infrared spectroscopy was performed on a Perkin Elmer Spectrum BX Fourier transform Infrared spectrometer (Perkin Elmer, Waltham, MA, USA). The dried samples of microgels were analyzed by observing various peaks for the different functional groups.

UV–visible spectroscopy. UV–visible spectroscopy was performed by using at a Shimadzu UV-2450 spectrometer was used for testing the UV–Vis spectroscopy. A temperature controller (TCC-240A) was equipped with it.

Thermo gravimetric analysis. By using a Shimadzu DTG-60H instrument, we analyzed all samples under nitrogen atmosphere (50 mL/min) at the heating rate of 10 °C/min.

Transmission electron microscopy (TEM). The morphology of the pure microgel and hybrid gels were studied by using transmission electron microscopy (TEM). For TEM sampling, microgels were diluted by distilled and then a sample drop was put on a stander copper grid supported by carbon film. The samples were dried at 50 °C and characterized by TEM with an accelerating voltage of 100 kV.

X-rays diffraction (XRD). The phase purity of Bimetallic nanoparticles was analyzed by X-ray diffraction (XRD) using a Bruker D2 PHASER X-ray Diffractometer with a graphite monochromator using Cu Kα radiation (λ = 1.54056 Å), operating at 30 kV and 15 mA.

X-rays photoelectron spectroscopy (XPS). The X-ray photoelectron spectroscopy (XPS) was performed on VG ESCALAB MKII spectrometer equipped with Al-Kα X-ray source.

Scanning electron microscopy (SEM). For SEM characterization, the samples were dropped on the silicon single crystal sheet, dried by IR light, which was carefully placed on conducting glue. Then all the samples were coated with gold vapor in order to become conducting and analyzed by JSM 6700F SEM.

Consent to publish. All co-authors are willing to publish the data in this journal.

Results and discussion

In this study, we were efficiently able to synthesis thio-functionalized poly N-isopropyl acrylamide microgels, which were impregnated by Copper Palladium and Cu/Pd nanoparticles successfully, as shown in Fig. 1. The carboxyl functionalized PNIPAM microgels were first prepared by soap-free emulsion polymerization. In polymerization, NIPAM acts as a temperature-sensitive monomer and acrylic acid used as a functional monomer. Then thiol group was introduced in the PNIPAM microgels by carbodiimide mediated reaction between the carboxyl group and 2-aminethanethiol (AET). The NPs of Cu, Pd and Cu/Pd Bimetallic were impregnated on thiol functionalized PNIPAM microgels particles. The color of the reaction mixture transformed instantaneously by the addition of reducing agent that indicated the formation of metallic nanoparticles (MNPs) into the microgels network. In-situ, the metallic NPs, were synthesized by the reduction of metal salt precursors having thermally tunable optical and excellent catalytic properties. The morphologies of pure microgel and Copper, Palladium

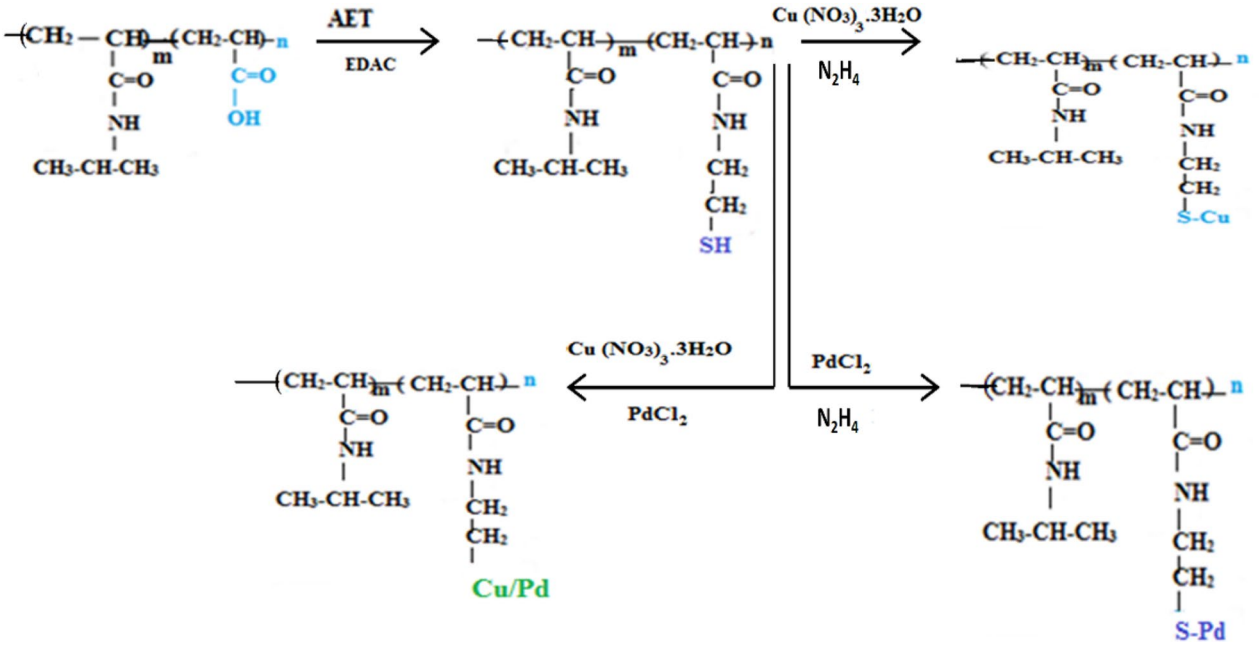

Figure 1. Schematic representation for the preparation of PNIPAM–K hybrid microgel.

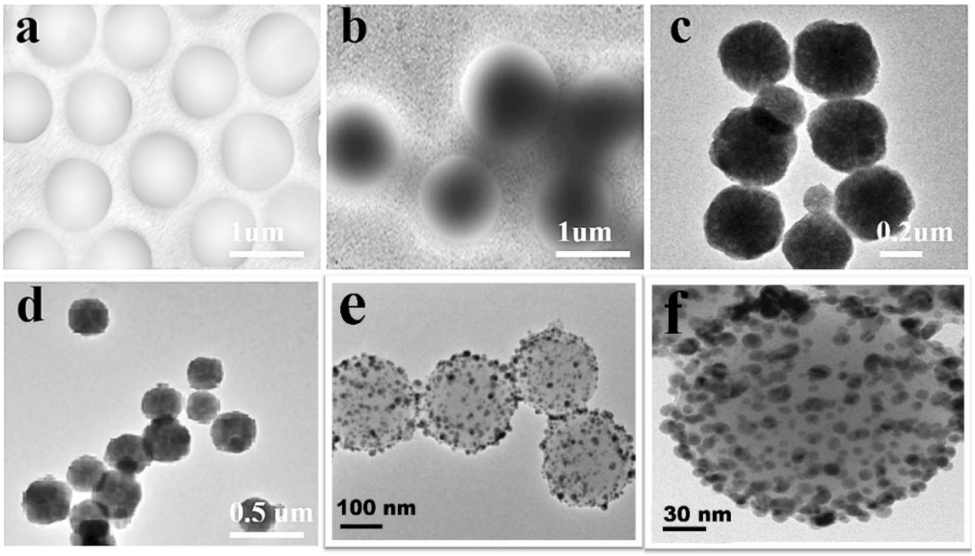

Figure 2. TEM images of (**a**) carboxyl-functionalized PNIPAM microgels, (**b**) thiol-functionalized PNIPAM microgels, (**c**) PNIPAM–Cu hybrid microgels (**d**) PNIPAM–Pd hybrid microgels and (**e**, **f**) Hexagonal core–shell nanoparticles of Cu/Pd.

based hybrid microgels were obtained by TEM, while the bi-metallic hybrid microgels were investigated by SEM, XRD and XPS.

The TEM photographs of the hybrid microgels showed that copper and palladium nanoparticles are uniformly distributed in the PNIPAM microgels and not aggregated, as shown in Fig. 2c,d. The average diameter of the Cu NPs is 6 ± 1 nm and that Pd NPs is 5 ± 1 nm. Similarly, the core–shell nanoparticles of Cu/Pd are visualized by SEM which shows hexagonal shapes as shown in Fig. 2.

To determine the oxidation states and surface compositions of the as prepared samples, X-ray photoelectron spectroscopy (XPS) characterization technique was employed. The Pd 3d and Cu 2p regions of the spectrum are given in Fig. 3a,b. Origin Pro 2019b software was used for XPS peaks fitting. Gaussian–Lorentzian function was employed for the peak fitting and Shirley type background correction was applied.

The binding energy in the range of 335–343 eV relating to the Pd 3d5/2 and 3d3/2 were observed in XPS spectra. The two intensive peaks as shown in Fig. 3a at 334.6 and 340.9 eV, confirmed the presence of metallic palladium (0). While the other doublets at 337.9 and 343.4 eV shows that palladium existence in its divalent state[48,49].

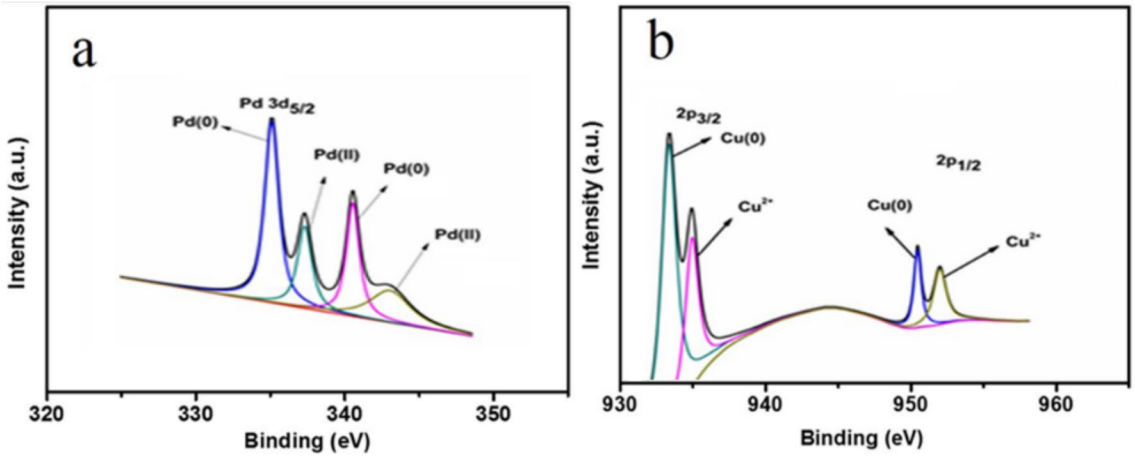

Figure 3. (**a**) XPS Spectra of Pd and (**b**) XPS spectra of copper. (OriginPro 2019b (64-bit) 9.6.5.169 version) https://downloadly.ir/software/engineering-specialized/originpro/.

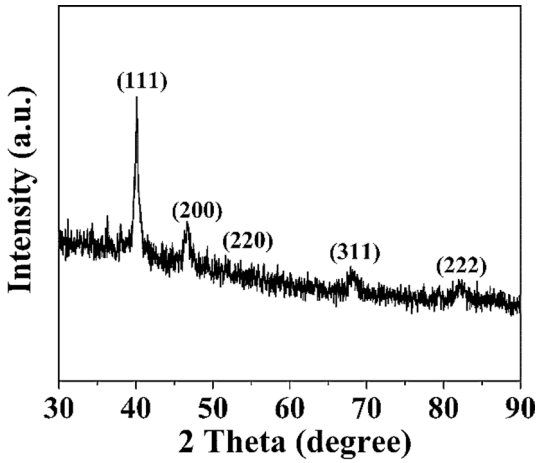

Figure 4. XRD Pattern for Copper palladium nanocrystal.

In the case of copper, it is challenging to differentiate Cu_2O from metallic Cu in the Cu 2p region of the XPS spectrum[50]. Although, the binding energies for Cu 2p3/2 were investigated in the XPS spectra at 932.2 eV and 934.6 eV, which confirmed the existence of copper in its both oxidation states (zero oxidation Cu (0) and divalent state Cu (II))[9]. Likewise, the binding energies for Cu 2p1/2 were also observed in the spectra at 951.0 and 953.1, which are representing Cu (0) and Cu (II), respectively as shown in Fig. 3b[50,51]. It can be seen that the oxidation states of Cu (0) are dominant than the Cu (II) values, which confirmed the presence of Cu in its metallic state[49]. Consequently, these findings confirmed that the palladium and copper nanoparticles are physically interacted with the surface of the hydrogel matrix.

The XRD studies of Cu/Pd hexagonal crystals are shown in Fig. 4. The diffracted peaks observed at 2θ value of 41°, 48°, 70°, 85°, and 90° correspond to the lattice plane (111), (200), (220), (311), and (222) respectively of CuPd (JCPDS card no. 48-1551) which shows resemblance with the SAED pattern as shown in Fig. 4.

FT-IR spectrum shown in Fig. 5 signifies the absorption peaks for amide I band at 1653, 1554, and 1381 cm^{-1} which is due to C=O stretching vibration[52,53]. The bending vibration of N–H, CH_3 and stretching vibration of C–N are collectively assigned to amide II band. The small peak shoulder at 1725 cm^{-1} represents the stretching vibration of C=O of the AA which produces a very dynamic o-acylisourea intermediate and reacts with strong nucleophile like primary amine to form amide bond. AET in the above reaction is used as a nucleophile to produce thiol group in the PNIPAM microgels. In the FT-IR spectrum for thiol-functionalized PNIPAM microgels (Fig. 5), the shoulder of the peak at 1725 cm^{-1} is very weak when compared with the carboxyl functionalized PNIPAM microgels (Fig. 5). Along with this, another weak peak at 2530 cm^{-1} represents the stretching band of S–H and a successful introduction of thiol group in the PNIPAM microgels[53,54]. In addition, the peaks at 1554 $cm^{-1}$and 1653 are both characteristic peaks of PNIPAM.

Thermo gravimetric analysis was performed to measure the thermal properties of hybrid microgels. We have only performed TG of thiol functionalized and copper hybrid microgels and compared the thermo gram of pure and copper hybrid microgels. It shows the difference between the degradation profile of pure and metals

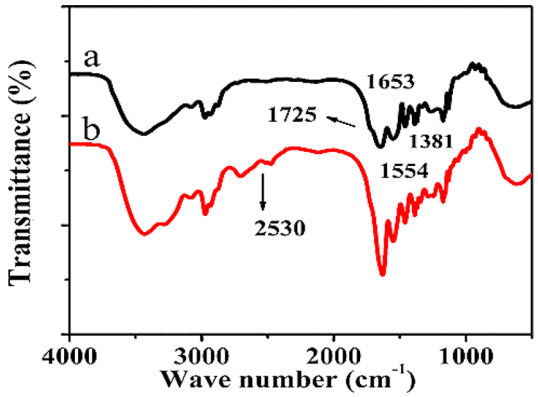

Figure 5. FT-IR spectra of (**a**) carboxyl-functionalized PNIPAM, and (**b**) thiol-functionalized PNIPAM microgels.

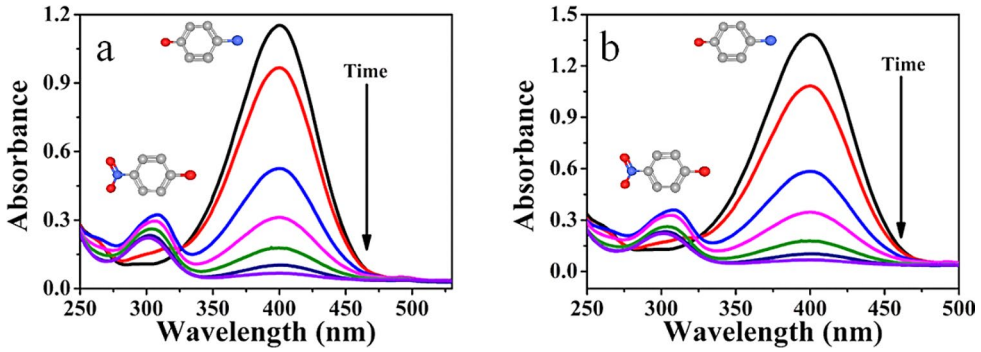

Figure 6. (**a**) Stepwise UV–Vis spectra of the reduction of 4-Nitrophenol catalyzed by NIPAM-Cu hybrid Microgels (**b**) by PNIPAM-Cu/Pd hybrid microgels.

encapsulated hybrid microgels from 30 to 600 °C. The weight of the PNIPAM-Cu hybrid microgels remained 55% of the original weight upon elevating the temperature up to 600 °C as shown in supporting information data Fig. S3. The TGA curve demonstrates the thermal stability of the hybrid microgels as compared to the thermo grams of the pure microgels. It is due to the encapsulation of metallic NPS in the microgels network. But the exact amount of the nanoparticles cannot be determined from it due to the formation of metallic oxides.

Catalytic performance of PNIPAM-Cu hybrid microgels. The catalytic activities of PNIPAM-Cu, PNIPAM-Pd and PNIPAM- Cu/Pd Bimetallic were probed by the reduction of 4-Nitrophenol (4-NP), and methylene blue with an excess volume of $NaBH_4$ as a sample reaction. For catalytic activity reactions, nitro compounds i.e. 4-Nitrophenol and dye methylene blue were used. The nitro compounds are very hazardous for health and are widely used in pharmaceutical products and dyes as well as pigments industries. A variety of pharmaceutical products like analgesics and antipyretics are obtained from nitro compounds. Excessive waste of nitro compounds causes many health and environmental issues[29,42]. The technique used for the reduction of these toxic compounds was UV–visible spectroscopy. It was experienced that aqueous solution of sodium borohydride gives recovered rate of reduction with catalyst. The rate of reduction is insignificant without catalyst due to the large potential difference between electron donor and acceptor species in excess reducing agents. So, the catalyst plays an imperative role to reduce the energy barrier in order to make it possible to reduce these products.

The reduction of 4-Nitrophenol and methylene blue were carried out in the presence of an excess amount of $NaBH_4$. The catalysts monometallic Cu, Pd and bimetallic Cu/Pd Hybrid accelerate the reduction reaction by transferring an electron from electron donor species BH_4^{-1} toelectron acceptor species i.e. 4-Nitrophenol. By using the catalyst, the 4-Nitrophenol was reduced by H ions of NaBH4 and converted into the 4-aminophenol, which is less toxic as compared with the 4-Nitrophenol. The rate of reduction of 4-Nitrophenol was monitored through UV–visible spectroscopy by calculating the decrease in the absorbance at 400 nm as given in Fig. 6, while on the same time the new peaks are prominent at 300 nm, which confirmed the presence of 4-aminophenol.

The rate of reduction of 4-Nitrophenol was studied at four different temperatures, i.e. 30 °C, 32 °C, 34 °C, 36 °C as shown in Fig. 7a. The kinetics of photo catalytic degradation of dyes can be depicted by first-order equation, which is given as follows;

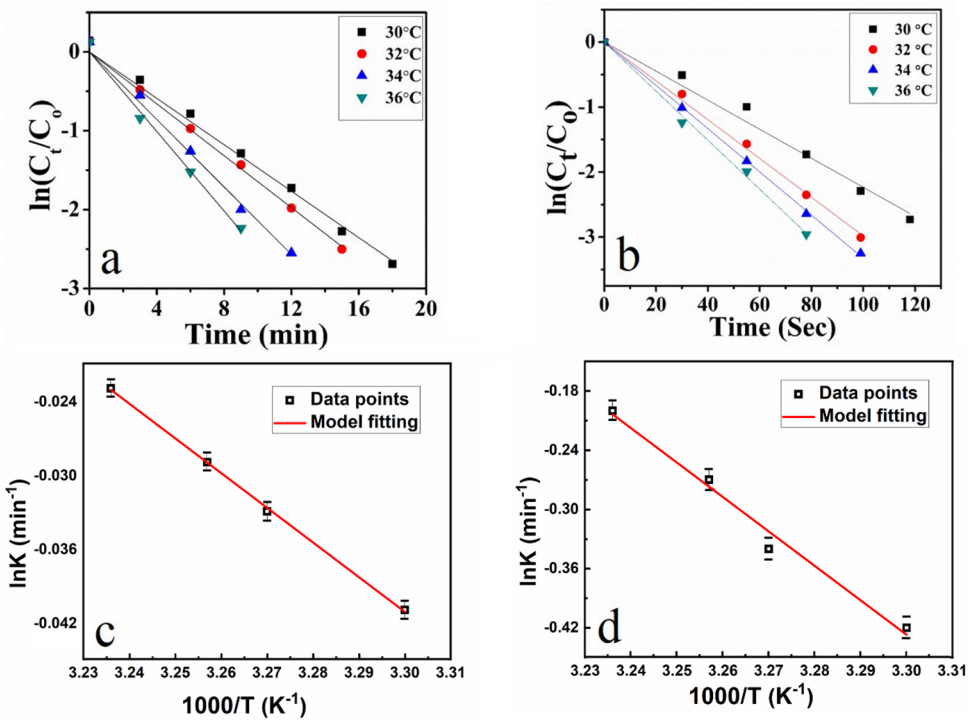

Figure 7. (**a**, **b**) Plot of ln (C_t/C_0) versus reaction time at a temperature of 30–36 °C for PNIPAM-Cu and PNIPAM-Cu/Pd respectively, where C_t is the concentration of 4-NP at time t and C_0 is the concentration of 4-NP at t = 0. (**c**) Plot of K_{app} versus temperature in the presence of Cu hybrid (**d**) plot of K_{app} versus temperature in the presence of bimetallic.

$$\ln\left(\frac{C_t}{C_0}\right) = K_{app}t$$

where K_{app}, C_o and C_t are the pseudo-first-order rate constant (min^{-1}), initial concentration of the dye, the concentration of dye solution at time *t* (min). The pseudo-first-order rate constant calculated from the slope of ln (C_t/C_0) vs time plot for different catalysts were found to be 0.11571.

The ln (C_t/C_0) determined from the UV–Vis spectra is plotted as a function of reaction time which determines "ln (C_t/C_0)" as shown in Fig. 7a,b. The plot of ln (C_t/C_0) versus time for reduction reaction indicates pseudo first-order kinetics. The slope of the curve at different temperatures shows that apparent rate constant (K_{app}) increases with increase in temperature, as shown in Fig. 7c,d. Increase in temperature increases the average kinetic energy and effective collisions of reactants (4-Nitrophenol, $NaBH_4$, microgels). So, the reduction rate of 4-Nitrophenol increased with increase in temperature.

The factors like temperature, nature and composition of metal hybrid on the rate of reduction of 4-Nitrophenol have been studied. It was observed by UV/Vis spectroscopy that bimetallic Cu/Pd hybrid microgels give a higher rate of reduction as compared to its atomic analogue as shown in Fig. 6b. The effect of temperature on the rate reduction of 4-Nitrophenol by bimetallic nanohybrid was also studied at four different temperatures i.e. 30 °C, 32 °C, 34 °C, 36 °C as shown in Fig. 7b. The rate of reduction of 4-Nitrophenol by PNIPAM/Pd hybrid microgels is nearly the same as PNIPAM/Cu hybrid microgels, as shown in Supplementary Fig. S1. The apparent rate constant from the slope of the curve at various temperatures followed pseudo first-order kinetics as shown in Fig. 7d. The reduction rate constant obtained from ln (C_t/C_0) vs time for 4-Nitrophenole at 30 °C by Cu and bimetallic Cu/Pd hybrid nanocomposites were 0.0223 min^{-1} and 0.223 min^{-1} respectively.

The reduction rate constant of 4-Nitrophenol by using bimetallic Cu/Pd nanocomposite is exceptionally greater than the rate of reduction of 4-Nitrophenol determined by other researchers reported in literature as shown in Table 1.

Correspondingly, the catalytic activities of PNIPAM-Cu/Pd, PNIPAM-Cu, and PNIPAM-Pd hybrid microgels were also investigated through the reduction of methylene blue in the presence of sufficient amount of $NaBH_4$ as a reducing agent at various temperatures (30–36 °C). The absorption peak of MB at 650 nm gradually reduced by the addition of PNIPAM-M catalysts, like PNIPAM-Cu/Pd, PNIPAM-Cu and PNIPAM-Pd hybrid microgels as shown in Fig. 8. From UV–visible spectra, ln (C_t/C_0) was calculated and plotted as a function of reaction time as shown in Fig. 9a,b and Fig. S2. This plot shows a linear relationship, which proves that the reduction reaction follows pseudo first-order kinetics (Fig. 8).

The apparent rate constants (Kapp) were calculated at various temperatures for all hybrid microgels. The Kapp increases with increase in temperature as observed from the slope of the curve for Cu hybrid and bimetallic Cu/

Nano catalyst	Kapp (min^{-1})	References
PNIPAM-Pd	0.082	[54]
AuNP/T-G hydrogel	0.0022	[55]
PVP-Pd	0.086	[54]
PNIPAM-AgNS	0.159	[53]
CN-supported PdNPs nanohybrids	9.5 × 10–5	[56]
MXene@PdNPs	0.003	[57]
Polyethyleneimine (PEI)/Polycaprolactone (PCL)@PdNPs	0.00276	[58]
Pd–Cu bimetallic nanomaterials (BNMs)	0.026	[43]
PNIPAM-Cu/Pd	0.223	**This work**

Table 1. Comparison of the PNIPAM-Cu/Pd catalyst with the literature reported catalysts for the 4-NP reduction.

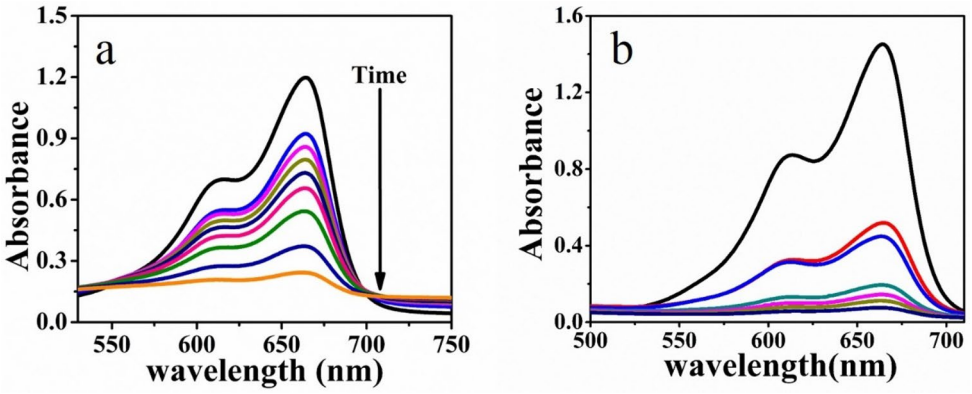

Figure 8. (**a**) Stepwise UV–Vis spectra of the reduction of MB catalyzed by PNIPAM-Cu hybrid microgels (**b**) by PNIPAM-Cu-Pd hybrid microgels.

Pd nanocomposites as shown in Fig. 9c,d. These catalytic activities are due to two factors i.e. diffusion rate and thermal properties of the catalytic reaction. As expected, different metals and their hybrids have different reaction activities. So, the Cu/Pd-PNIPAM was found to have the highest catalytic activities as compare to PNIPAM-Cu and PNIPAM-Pd. The improved catalytic efficiency of bimetallic Cu/Pd nanocomposites for the reduction of methylene blue was observed as compared to the recently published literature (Table 2).

In-situ the metallic nanoparticles Cu, Pd and Cu/Pd nanoparticles were synthesized in PNIPAM microgels by the reduction of metals salts precursors in the presence of thiol-functionalized microgels and hydrazine hydrate. The localized surface resonance band was observed at 600 nm for copper hybrid microgels. Increase in temperature decreases the size and inter particle distance which increases the refractive index and causes red shift of local resonance band for Cu Nanoparticles as shown in Fig. 10a,b. The red shift becomes larger with increasing temperature from 25 to 55 °C, which broadened the LSPR band gradually. Whereas the Plasmon coupling of the approaching particles causes red shifting due to decrease of band intensity.

Conclusion

By using the soap-free emulsion polymerization, the thiol functionalized PNIPAM microgel was prepared, which was used for the in situ preparation of nanocomposites impregnated with metals such as copper, palladium and copper palladium alloy. The Copper Palladium Alloy nanocomposites have shown excellent catalytic properties by degrading Nitro phenol and methylene blue in the presence of $NaBH_4$. This high catalytic performance is due to the hydrogels network which provided stability for metal nanoparticles. SEM and TEM images showed that metal nanoparticles in the microgels network have no aggregation. The PNIPAM microgels with the functionalization of thiol group were obtained by developing an amide bond between AET and carboxyl-functionalized PNIPAM microgel. The main significance of this protocol is that the thiol group and MNPs distribution can be controlled by the carboxyl group within the PNIPAM microgels backbone. It is due to the presence of carboxyl containing monomers having specific reactivity ratios.

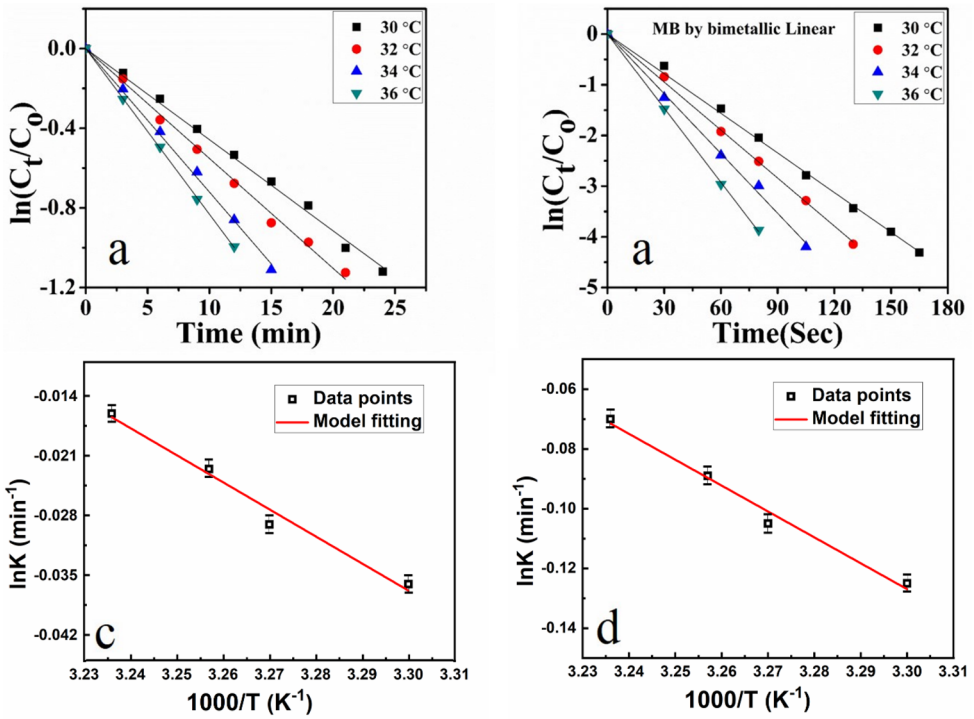

Figure 9. (**a**, **b**) Plot of ln (C_t/C_0) versus reaction time at a temperature of 30–36 °C for PNIPAM-Cu and PNIPAM-Cu/Pd respectively, where C_t is the concentration of MB at time t and C_0 is the concentration of MB at t = 0. (**c**, **d**) Plot of lnkapp versus temperature for Cu hybrid and bimetallic nanocomposites respectively.

Catalyst	Kapp (min^{-1})	References
Ag-NP	0.182	[59]
p(EP-g-AA)-Cu	0.04151	[60]
QAMPS/VP-Fe_3O_4 QAMPS	0.0032	[61]
Fe_3O_4 QAMPS/VP-Ag	0.0053	[61]
PNIPAM-Cu/Pd	0.173	**This work**

Table 2. Comparison of the PNIPAM-Cu/Pd catalyst with the literature reported catalysts for the MB reduction.

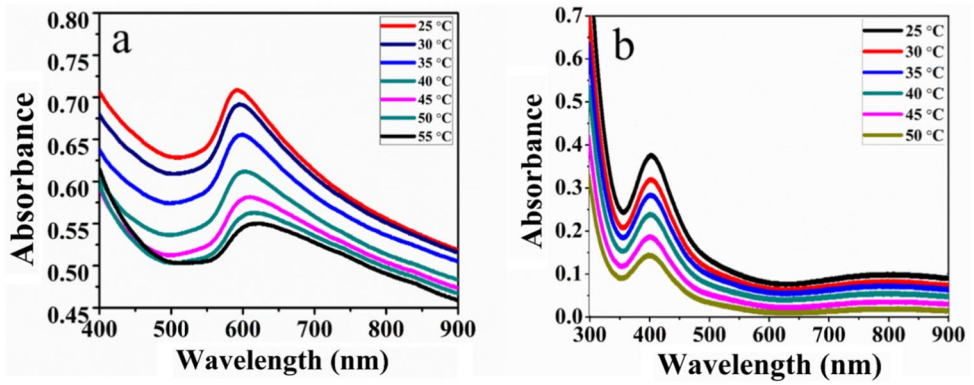

Figure 10. (**a**) Effect of temperature on the UV–Vis spectra of PNIPAM-Cu hybrid microgels and (**b**) PNIPAM-Cu/Pd hybrid microgels.

Received: 26 January 2021; Accepted: 5 July 2021
Published online: 20 July 2021

References

1. Zuraiqi, K. *et al.* Liquid metals in catalysis for energy applications. *Joule* **4**, 2290–2321 (2020).
2. Franz, K. J. & Metzler-Nolte, N. Introduction: Metals in medicine. *Chem. Rev.* **119**, 727–729 (2019).
3. Yin, J., Hu, Y. & Yoon, J. Fluorescent probes and bioimaging: Alkali metals, alkaline earth metals and pH. *Chem. Soc. Rev.* **44**, 4619–4644 (2015).
4. Aragay, G. & Merkoçi, A. Nanomaterials application in electrochemical detection of heavy metals. *Electrochim. Acta* **84**, 49–61 (2012).
5. Dickey, M. D. Stretchable and soft electronics using liquid metals. *Adv. Mater.* **29**, 1606425 (2017).
6. Tang, C. *et al.* Towards efficient use of noble metals: Via exsolution exemplified for CO oxidation. *Nanoscale* **11**, 16935–16944 (2019).
7. Esconjauregui, S., Whelan, C. M. & Maex, K. The reasons why metals catalyze the nucleation and growth of carbon nanotubes and other carbon nanomorphologies. *Carbon NY.* **47**, 659–669 (2009).
8. Huang, F., Liu, Z. & Yu, Z. C-Alkylation of ketones and related compounds by alcohols: Transition-metal-catalyzed dehydrogenation. *Angew. Chemie Int. Ed.* **55**, 862–875 (2016).
9. Xu, C., Liu, Y., Wang, J., Geng, H. & Qiu, H. Nanoporous PdCu alloy for formic acid electro-oxidation. *J. Power Sources* **199**, 124–131 (2012).
10. Li, H., Yang, P., Pageni, P. & Tang, C. Recent advances in metal-containing polymer hydrogels. *Macromol. Rapid Commun.* **38**, 1700109 (2017).
11. Scott, R. W. J., Wilson, O. M. & Crooks, R. M. Synthesis, characterization, and applications of dendrimer-encapsulated nanoparticles. *J. Phys. Chem. B* **109**, 692–704 (2005).
12. Hamley, I. W. Nanostructure fabrication using block copolymers. *Nanotechnology* **14**, R39 (2003).
13. Vishwanath, V. & Rao, H. Gutta-percha in endodontics—A comprehensive review of material science. *J. Conserv. Dent.* **22**, 216 (2019).
14. Dizaj, S. M., Mennati, A., Jafari, S., Khezri, K. & Adibkia, K. Antimicrobial activity of carbon-based nanoparticles. *Adv. Pharm. Bull.* **5**, 19–23 (2015).
15. Roy, I. *et al.* Ceramic-based nanoparticles entrapping water-insoluble photosensitizing anticancer drugs: A novel drug-carrier system for photodynamic therapy. *J. Am. Chem. Soc.* **125**, 7860–7865 (2003).
16. Gold, K., Slay, B., Knackstedt, M. & Gaharwar, A. K. Antimicrobial activity of metal and metal-oxide based nanoparticles. *Adv. Ther.* **1**, 1700033 (2018).
17. Gaharwar, A. K., Dammu, S. A., Canter, J. M., Wu, C. J. & Schmidt, G. Highly extensible, tough, and elastomeric nanocomposite hydrogels from poly(ethylene glycol) and hydroxyapatite nanoparticles. *Biomacromol* **12**, 1641–1650 (2011).
18. Skelton, S. *et al.* Biomimetic adhesive containing nanocomposite hydrogel with enhanced materials properties. *Soft Matter* **9**, 3825–3833 (2013).
19. Vashist, A. *et al.* Nanocomposite hydrogels: Advances in nanofillers used for nanomedicine. *Gels* **4**, 75 (2018).
20. Liu, Z. *et al.* Nanocomposite smart hydrogels with improved responsiveness and mechanical properties: A mini review. *J. Polym. Sci. Part B Polym. Phys.* **56**, 1306–1313 (2018).
21. Adewunmi, A. A., Ismail, S. & Sultan, A. S. Carbon nanotubes (CNTs) Nanocomposite hydrogels developed for various applications: A critical review. *J. Inorg. Organomet. Polym Mater.* **26**, 717–737 (2016).
22. Karimi, A. & Wan Daud, W. M. A. Materials, preparation, and characterization of PVA/MMT nanocomposite hydrogels: A review. *Polym. Compos.* **38**, 1086–1102 (2017).
23. Choi, J. *et al.* Preparation and characterization of graphene oxide supported Cu, Cu2O, and CuO nanocomposites and their high photocatalytic activity for organic dye molecule. *Curr. Appl. Phys.* **17**, 137–145 (2017).
24. Sargin, I., Baran, T. & Arslan, G. Environmental remediation by chitosan-carbon nanotube supported palladium nanoparticles: Conversion of toxic nitroarenes into aromatic amines, degradation of dye pollutants and green synthesis of biaryls. *Sep. Purif. Technol.* **247**, 116987 (2020).
25. Rambabu, K., Bharath, G., Banat, F. & Show, P. L. Green synthesis of zinc oxide nanoparticles using Phoenix dactylifera waste as bioreductant for effective dye degradation and antibacterial performance in wastewater treatment. *J. Hazard. Mater.* **402**, 123560 (2021).
26. Hu, H. *et al.* Synthesis and stabilization of metal nanocatalysts for reduction reactions—A review. *J. Mater. Chem.* **A3**, 11157–11182 (2015).
27. Sarkar, A. K. *et al.* Cross-linked biopolymer stabilized exfoliated titanate nanosheet-supported AgNPs: A green sustainable ternary nanocomposite hydrogel for catalytic and antimicrobial activity. *ACS Sustain. Chem. Eng.* **5**, 1881–1891 (2017).
28. Li, X. *et al.* Cellulosic protic ionic liquids hydrogel: A green and efficient catalyst carrier for Pd nanoparticles in reduction of 4-nitrophenol in water. *Chem. Eng. J.* **372**, 516–525 (2019).
29. Khalil, A., Ali, N., Khan, A., Asiri, A. M. & Kamal, T. Catalytic potential of cobalt oxide and agar nanocomposite hydrogel for the chemical reduction of organic pollutants. *Int. J. Biol. Macromol.* **164**, 2922–2930 (2020).
30. Maijan, P., Amornpitoksuk, P. & Chantarak, S. Synthesis and characterization of poly(vinyl alcohol-g-acrylamide)/SiO2@ZnO photocatalytic hydrogel composite for removal and degradation of methylene blue. *Polymer (Guildf).* **203**, 122771 (2020).
31. Ismail, M. *et al.* Pollution, toxicity and carcinogenicity of organic dyes and their catalytic bio-remediation. *Curr. Pharm. Des.* **25**, 3645–3663 (2019).
32. Yue, Y., Wang, X., Wu, Q., Han, J. & Jiang, J. Highly recyclable and super-tough hydrogel mediated by dual-functional TiO_2 nanoparticles toward efficient photodegradation of organic water pollutants. *J. Colloid Interface Sci.* **564**, 99–112 (2020).
33. Haleem, A. *et al.* Hybrid cryogels composed of P(NIPAM-co-AMPS) and metal nanoparticles for rapid reduction of p-nitrophenol. *Polymer (Guildf).* **193**, 122352 (2020).
34. Din, M. I. *et al.* Nanocatalytic assemblies for catalytic reduction of nitrophenols: A critical review. *Crit. Rev. Anal. Chem.* **50**, 322–338 (2020).
35. Van Tran, V., Park, D. & Lee, Y. C. Hydrogel applications for adsorption of contaminants in water and wastewater treatment. *Environ. Sci. Pollut. Res.* **25**, 24569–24599 (2018).
36. Sinha, V. & Chakma, S. Advances in the preparation of hydrogel for wastewater treatment: A concise review. *J. Environ. Chem. Eng.* **7**, 103295 (2019).
37. Zhang, Z. *et al.* Bifunctional nanocatalyst based on three-dimensional carbon nanotube-graphene hydrogel supported Pd nanoparticles: One-pot synthesis and its catalytic properties. *ACS Appl. Mater. Interfaces* **6**, 21035–21040 (2014).
38. Zheng, Y. & Wang, A. Ag nanoparticle-entrapped hydrogel as promising material for catalytic reduction of organic dyes. *J. Mater. Chem.* **22**, 16552–16559 (2012).
39. Wu, X. Q., Wu, X. W., Huang, Q., Shen, J. S. & Zhang, H. W. In situ synthesized gold nanoparticles in hydrogels for catalytic reduction of nitroaromatic compounds. *Appl. Surf. Sci.* **331**, 210–218 (2015).

40. Naseem, K., Begum, R. & Farooqi, Z. H. Catalytic reduction of 2-nitroaniline: A review. *Environ. Sci. Pollut. Res.* **24**, 6446–6460 (2017).
41. Yuan, M. *et al.* Bimetallic PdCu nanoparticle decorated three-dimensional graphene hydrogel for non-enzymatic amperometric glucose sensor. *Sens. Actuators B Chem.* **190**, 707–714 (2014).
42. Xu, Z. *et al.* Catalytic reduction of 4-nitrophenol over graphene supported Cu@Ni bimetallic nanowires. *Mater. Chem. Phys.* **227**, 64–71 (2019).
43. Zhan, F. *et al.* Controllable morphology and highly efficient catalytic performances of Pd–Cu bimetallic nanomaterials prepared via seed-mediated co-reduction synthesis. *Appl. Surf. Sci.* **527**, 146719 (2020).
44. Wang, Y. *et al.* One-pot green synthesis of bimetallic hollow palladium–platinum nanotubes for enhanced catalytic reduction of p-nitrophenol. *J. Colloid Interface Sci.* **539**, 161–167 (2019).
45. Fang, W. *et al.* Synthesis of Pd/Au bimetallic nanoparticle-loaded ultrathin graphitic carbon nitride nanosheets for highly efficient catalytic reduction of p-nitrophenol. *J. Colloid Interface Sci.* **490**, 834–843 (2017).
46. Wu, Y. *et al.* Carbon-nanotube-doped Pd-Ni bimetallic three-dimensional electrode for electrocatalytic hydrodechlorination of 4-chlorophenol: Enhanced activity and stability. *J. Hazard. Mater.* **356**, 17–25 (2018).
47. Begum, R., Rehan, R., Farooqi, Z. H., Butt, Z. & Ashraf, S. Physical chemistry of catalytic reduction of nitroarenes using various nanocatalytic systems: Past, present, and future. *J. Nanopart. Res.* **18**, 1–24 (2016).
48. Wang, X. *et al.* The synergy between atomically dispersed Pd and cerium oxide for enhanced catalytic properties. *Nanoscale* **9**, 6643–6648 (2017).
49. Göksu, H., Zengin, N., Burhan, H., Cellat, K. & Şen, F. A novel hydrogenation of nitroarene compounds with multi wall carbon nanotube supported palladium/copper nanoparticles (PdCu@MWCNT NPs) in aqueous medium. *Sci. Rep.* **10**, 1–8 (2020).
50. Larrazábal, G. O., Martín, A. J., Mitchell, S., Hauert, R. & Pérez-Ramírez, J. Enhanced reduction of CO_2 to CO over Cu–In electrocatalysts: Catalyst evolution is the key. *ACS Catal.* **6**, 6265–6274 (2016).
51. Rajesh, U. C., Pavan, V. S. & Rawat, D. S. Copper NPs supported on hematite as magnetically recoverable nanocatalysts for a one-pot synthesis of aminoindolizines and pyrrolo[1,2-a]quinolines. *RSC Adv.* **6**, 2935–2943 (2016).
52. Ul Haq, I. *et al.* Highly efficient separation of 1,3-butadiene from nitrogen mixture by adsorption on highly stable MOF. *Chem. Eng. J.* **402**, 125980 (2020).
53. Satapathy, S. S. *et al.* Thermo-responsive PNIPAM-metal hybrids: An efficient nanocatalyst for the reduction of 4-nitrophenol. *Appl. Surf. Sci.* **420**, 753–763 (2017).
54. Wang, Q., Wang, J., Wang, D., Turhong, M. & Zhang, M. Recyclable and effective Pd/poly(N-isopropylacrylamide) catalyst for hydrodechlorination of 4-chlorophenol in aqueous solution. *Chem. Eng. J.* **280**, 158–164 (2015).
55. Zhu, J. *et al.* A facile preparation method for new two-component supramolecular hydrogels and their performances in adsorption, catalysis, and stimuli-response. *RSC Adv.* **9**, 22551–22558 (2019).
56. Lebaschi, S., Hekmati, M. & Veisi, H. Green synthesis of palladium nanoparticles mediated by black tea leaves (*Camellia sinensis*) extract: Catalytic activity in the reduction of 4-nitrophenol and Suzuki-Miyaura coupling reaction under ligand-free conditions. *J. Colloid Interface Sci.* **485**, 223–231 (2017).
57. Yin, J. *et al.* Highly effcient catalytic performances of nitro compounds and morin via self-assembled mxene-pd nanocomposites synthesized through self-reduction strategy. *Nanomaterials* **9**, https://doi.org/10.3390/nano9071009 (2019).
58. Wang, C. *et al.* Preparation of palladium nanoparticles decorated polyethyleneimine/polycaprolactone composite fibers constructed by electrospinning with highly efficient and recyclable catalytic performances. *Catalysts* **9**, 559 (2019).
59. Indana, M. K., Gangapuram, B. R., Dadigala, R., Bandi, R. & Guttena, V. A novel green synthesis and characterization of silver nanoparticles using gum tragacanth and evaluation of their potential catalytic reduction activities with methylene blue and Congo red dyes. *J. Anal. Sci. Technol.* **7**, 19 (2016).
60. Su, R. *et al.* Biomass-based soft hydrogel for triple use: Adsorbent for metal removal, template for metal nanoparticle synthesis, and a reactor for nitrophenol and methylene blue reduction. *J. Taiwan Inst. Chem. Eng.* **91**, 235–242 (2018).
61. Atta, A. M., Moustafa, Y. M., Al-Lohedan, H. A., Ezzat, A. O. & Hashem, A. I. Methylene blue catalytic degradation using silver and magnetite nanoparticles functionalized with a poly(ionic liquid) based on quaternized dialkylethanolamine with 2-acrylamido-2-methylpropane sulfonate-co-vinylpyrrolidone. *ACS Omega*. https://doi.org/10.1021/acsomega.9b03610 (2020).

Acknowledgements

We are thankful for the support of the Innovation Foundation of Radiation Application, China, as they have funded this project under the project number (KFZC2018040208). Taif University Researchers Supporting Project Number (TURSP-2020/140), Taif University, Taif, Saudi Arabia.

Author contributions

We declare that this work was done by the authors named in this article, and all liabilities pertaining to claims relating to the content of this article will be borne by the authors. M.U.K., K.K. and M.A. generate the idea and perform the experimental work. R.S., E.K., A.H. and I.I. analysis the data and writing the manuscript, M.H. perform the proof reading, Y.D., R.D. provide all the funding and guidelines for the manuscript.

Competing interests

The authors declare no competing interests.

Additional information

Supplementary Information The online version contains supplementary material available at https://doi.org/10.1038/s41598-021-94177-6.

Correspondence and requests for materials should be addressed to R.S. or R.D.

Reprints and permissions information is available at www.nature.com/reprints.

Publisher's note Springer Nature remains neutral with regard to jurisdictional claims in published maps and institutional affiliations.

Open Access This article is licensed under a Creative Commons Attribution 4.0 International License, which permits use, sharing, adaptation, distribution and reproduction in any medium or format, as long as you give appropriate credit to the original author(s) and the source, provide a link to the Creative Commons licence, and indicate if changes were made. The images or other third party material in this article are included in the article's Creative Commons licence, unless indicated otherwise in a credit line to the material. If material is not included in the article's Creative Commons licence and your intended use is not permitted by statutory regulation or exceeds the permitted use, you will need to obtain permission directly from the copyright holder. To view a copy of this licence, visit http://creativecommons.org/licenses/by/4.0/.

© The Author(s) 2021